https://doi.org/10.5194/egusphere-2025-2990
Preprint. Discussion started: 1 August 2025


# Cross–Seasonal Impact of SST Anomalies over the Tropical Central Pacific Ocean on the Antarctic Stratosphere

Yucheng Zi[1,2,3,4], Zhenxia Long[3], Jinyu Sheng[2], Gaopeng Lu[1], Will Perrie[2,3,5], and Ziniu Xiao[1,4]

*Correspondence*: Zhenxia Long (Zhenxia.Long@dfo-mpo.gc.ca) and Ziniu. Xiao (xiaozn@lasg.iap.ac.cn)

[1] School of Earth and Space Sciences, University of Science and Technology of China, Hefei, China

[2] Department of Oceanography, Dalhousie University, Halifax, Nova Scotia, Canada

[3] Fisheries and Oceans Canada, Bedford Institute of Oceanography, Dartmouth, Nova Scotia, Canada

[4] State Key Laboratory of Earth System Numerical Modeling and Application, Institute of Atmospheric Physics, Chinese Academy of Sciences, Beijing, China

[5] Department of Engineering Mathematics & Internetworking, Dalhousie University, Halifax, Canada

https://doi.org/10.5194/egusphere-2025-2990
Preprint. Discussion started: 1 August 2025


**Abstract**

In this study we examine the cross–seasonal effects of boreal winter sea surface temperature (SST) anomalies over the central tropical Pacific (Niño4 region) on Antarctic stratospheric circulation and ozone transport during the subsequent austral winter using ERA5 reanalysis of 45 years (1980–2024). Our analyses show that warm (cold) SST anomalies in Niño4 region during December–February are associated with polar stratospheric warming (cooling), a weakened (strengthened) stratospheric polar vortex (SPV), and enhanced (suppressed) polar ozone concentrations during July–September of the subsequent year. This delayed response is mediated by a Pacific–South America (PSA) teleconnection, which excites planetary waves that propagate upward into stratosphere and modify the Brewer–Dobson circulation. In addition, as the influence of Niño4 SSTs on the PSA teleconnection pattern diminishes during July-September, surface heat feedback at mid and high latitudes becomes critically important for planetary waves. Specifically, persistent South Pacific SST warming and sea-ice loss over the Amundsen and Ross Seas reinforce planetary waves by releasing heat from ocean into atmosphere. A multivariate regression statistical model using predictors of boreal winter Niño4 SST, June PSA, June South Pacific SST, and May–June sea-ice concentration (SIC) indices explain approximately 35 % of the variance in austral winter stratospheric temperatures. These findings highlight a previously underexplored pathway through which tropical Pacific SST anomalies modulate Antarctic stratospheric dynamics and chemistry on seasonal timescales. This implies a new insight into tropical–polar coupling and provides a potential signal for extended–range forecasts of ozone depletion risk.

**Keywords:** El Niño–Southern Oscillation (ENSO); Stratospheric warming; Stratospheric polar vortex (SPV); Antarctic ozone; Pacific–South America (PSA) pattern; Multivariate regression

https://doi.org/10.5194/egusphere-2025-2990
Preprint. Discussion started: 1 August 2025


## 1 Introduction

The Antarctic stratospheric circulation is largely governed by the wintertime Stratospheric Polar Vortex (SPV), which is a major driver of weather and climate variability across the Southern Hemisphere (Baldwin et al., 2021). Compared to its Northern Hemisphere counterpart, the Antarctic SPV is generally more stable, owing to weaker thermal contrasts between the ocean and land. Despite this stability, the Antarctic SPV exhibits considerable interannual variability (Domeisen et al., 2019; Baldwin et al., 2021). Furthermore, the Antarctic stratosphere plays a crucial role in modulating weather and climate in the Southern Hemisphere through the seasonal evolution of SPV and its dynamics processes and interaction with ozone chemistry (Thompson et al., 2005; Solomon et al., 2016).

Previous studies revealed large interannual variations and long-term trends in the SPV, stratospheric temperatures, and ozone concentrations (Karpetchko et al., 2005). In the late 20th century, anthropogenic emissions of chlorofluorocarbons (CFCs) cooled the polar stratosphere, intensified the SPV, and caused severe springtime ozone depletion, which resulted in the formation of the Antarctic ozone hole (Solomon et al., 2016). After the implementation of the Montreal Protocol for phasing out production and consumption of ozone-depleting substances, signs of ozone recovery have emerged, accompanied by a gradual weakening of the SPV and associated stratospheric warming (Solomon et al., 2016). Superimposed on the long-term trends of SPV are substantial interannual variations and extreme events. For instance, exceptionally weak SPV episodes triggered by sudden stratospheric warmings (SSWs) occurred respectively in 2002, 2010, 2019, and 2024 (Thompson and Solomon, 2002; Esler et al., 2006; Laat and Weele 2011; Shen et al., 2020; Zi et al., 2025), and an unusually strong SPV event driven by the pronounced ozone depletion occurred in 2020 (Lim et al., 2024).

Several natural factors contribute to the above-mentioned SPV variability. The phase of the Quasi-Biennial Oscillation (QBO), for instance, modulates planetary-wave propagation and can either strengthen or weaken the SPV (Kuroda et al., 2007). El Niño–Southern Oscillation (ENSO) events also leave distinct warm- and cold-year signatures on Antarctic stratospheric temperatures and ozone through changes in tropospheric wave forcing and the Brewer–Dobson (B-D) circulation (Yang et al., 2015; Stone et al., 2022; Rao et al., 2023; Wang et al., 2025). In addition, solar-cycle variability contributes to interannual modulation by altering ultraviolet irradiance and stratospheric

https://doi.org/10.5194/egusphere-2025-2990
Preprint. Discussion started: 1 August 2025


heating rates (Kuroda et al., 2007). Alongside these natural drivers, fluctuations in the atmospheric burdens of ozone-depleting substances and greenhouse gases continue to influence both the magnitude and nature of Antarctic stratospheric variability (Singh and Bhargawa, 2019).

ENSO is the most prominent mode of interannual climate variability (Wang, 2018). Developing in boreal autumn and peaking in winter, ENSO influences the global weather patterns through atmospheric teleconnections (McPhaden et al., 2006). It also modulates the SPV primarily via the Pacific–North America (PNA) and Pacific–South America (PSA) wave trains (Garfinkel and Hartmann, 2008; Ineson and Scaife, 2009; Barriopedro and Calvo, 2014; Polvani et al., 2017; Song and Son, 2018; Zhang et al., 2022). In the Northern Hemisphere, El Niño events enhance tropical convection and amplify the PNA pattern, strengthening the Aleutian Low, which in turn increases upward wave activity and weakens the SPV (Garfinkel and Hartmann, 2008; Butler and Polvani, 2011; Zhang et al., 2022). In the Southern Hemisphere, central Pacific (CP–type) El Niño events during September–February enhance convection near the South Pacific Convergence Zone (SPCZ), which triggers the PSA wave trains that can weaken the Antarctic SPV, resulting in stratospheric warming and ozone enhancement (Hurwitz et al., 2011a,b; Yang et al., 2015; Manatsa and Mukwada, 2017; Domeisen et al., 2019; Ma et al., 2022). In contrast, Eastern Pacific (EP–type) El Niño events were found to produce weaker stratospheric responses (Hurwitz et al., 2011a; Zubiaurre and Calvo, 2012).

Although many studies were made on the Antarctic stratosphere's simultaneous or 1-2 months lag responses to ENSO from September to February (L'Heureux and Thompson, 2006; Silvestri and Vera, 2009; Hu and Fu, 2010; Fogt et al., 2011; Lin et al., 2012; Kim et al., 2017; Ma et al., 2022), our knowledge remains very limited on the ENSO's cross–seasonal and delayed effects (Manatsa and Mukwada, 2017; Niu et al., 2023). Some previous studies found that delayed ozone responses occur in the year following an ENSO event (Lin and Qian, 2019), while others suggested that tropical sea surface temperature (SST) anomalies as early as June can influence stratospheric circulation later in the year (Grassi et al., 2008; Evtushevsky et al., 2015; Lim et al., 2018; Stone et al., 2022). Yang et al. (2015) examined correlations between ENSO and Antarctic stratospheric temperatures during July–September, but these were primarily interpreted as concurrent responses. Despite these studies, the physical mechanisms by which ENSO events in boreal winter influence the Antarctic stratosphere during the following austral winter (July–September) remain poorly

https://doi.org/10.5194/egusphere-2025-2990
Preprint. Discussion started: 1 August 2025


understood. Better understanding of ENSO's delayed impact is particularly important, since the SPV in the austral winter is strongest and most susceptible to dynamical disturbances, with significant implications for polar ozone chemistry (Lin et al., 2009; Thompson et al., 2011).

The main objective of this study is to examine how the boreal winter SST anomalies (SSTs) influence the Antarctic stratosphere during the following austral winter, with a special emphasis on mechanisms by which Niño4 SSTs modulate polar stratospheric dynamics and ozone transport, and associated planetary wave propagation and mid-latitude sea-air interactions. A muti-regression analysis will also be used to evaluate the potential for predicting stratospheric temperature anomalies based on early–season climate indicators. The structure of this paper is as follows. Section 2 describes the data and methodology. Section 3 presents quantification of the ENSO–Antarctic stratosphere relationship. Section 4 shows an examination of the underlying dynamical mechanisms. Section 5 presents the multivariate regression analysis. Section 6 is a summary and conclusion.

## 2. Data and methods

### 2.1 Data

The 6-hourly and monthly-mean atmospheric variables in the 45-year period 1980–2024 extracted from the ERA5 reanalysis (Hersbach et al., 2023a,b) are used in this study. This reanalysis with a horizontal resolution of 1°×1° was generated by the European Centre for Medium-Range Weather Forecasts (ECMWF). These atmospheric variables at 37 vertical pressure levels include the geopotential height, horizontal and vertical winds, temperature, sea level pressure (SLP), ozone mass mixing ratio, total column ozone (TCO3), net surface downward short-wave radiation flux, net surface upward long-wave radiation flux, latent and sensible heat fluxes, outgoing long-wave radiation flux (OLR). The monthly sea surface temperature (SST) and sea-ice concentration (SIC) during the same study period were also extracted from ERA5 reanalysis.

Several indices (such as Niño3, Niño3.4, and Niño4) based on SST anomalies averaged over a given region have been used to monitor the dynamic activities in the tropic Pacific (Bamston et al. 1997; Trenberth, 1997). Niño 3 is the SST anomalies averaged over the region between 5 °N and 5 °S and between 150 °W and 90 °W, and has been used for monitoring and predicting El Niño and La Niña events (Trenberth, 1997). Niño 3.4 is the SST anomalies averaged over the region

https://doi.org/10.5194/egusphere-2025-2990
Preprint. Discussion started: 1 August 2025


between 5 °N–5 °S and 170 °W–120 °W, and has been used as the primary index for monitoring ENSO due to its ability to capture basin-scale variability (Bamston et al. 1997). Niño 4 is the SST anomalies averaged over the region between 5 °N–5 °S and 160 °W–150 °W, which is to monitor SST anomalies in the central equatorial Pacific. In this study, the SST indices for Niño3, Niño3.4, and Niño4 were obtained from the HadISST1.1 dataset (Rayner et al., 2003).

The Pacific–South America pattern (PSA) index was used to examine stratosphere and troposphere interactions, which was derived by projecting area–weighted SLP anomalies south of 20 °S onto the second Empirical Orthogonal Function (EOF) mode (Mo and Higgins, 1998). All anomalies are calculated relative to the 1991–2020 daily and monthly climatology, and all data have been detrended. Statistical significance is assessed using the Student t-test.

## 2.2 Method

### 2.2.1 E–P flux

The Eliassen–Palm (E–P) theorem is used to diagnose interactions between eddies and the zonal–mean flow in both the stratosphere and troposphere (Andrews et al., 1987). The E–P flux ($\vec{F}$) and its divergence ($\nabla \cdot \vec{F}$) are defined:

$$\vec{F} = \left(\vec{F}_{\varphi}, \vec{F}_{p}\right) = r_0 cos\varphi \left\{ - [u'v'], \frac{f}{[\theta_p]} [v'\theta'] \right\} \quad (1)$$

$$\nabla \cdot \vec{F} = \frac{1}{r_0 \cos\varphi} \frac{\partial}{\partial \varphi} \left(\vec{F}_{\varphi} \cos\varphi\right) + \frac{\partial}{\partial p} \left(\vec{F}_{p}\right) \quad (2)$$

where $u$ and $v$ are the zonal and meridional wind components, respectively, and $\theta$ is the potential temperature. $\varphi$ and $p$ denote latitude and pressure, respectively. $f$ is the Coriolis parameter, and $r_0$ is Earth's radius. Square brackets [ ] indicate zonal averages, and primes (′) denote deviations from the zonal mean.

### 2.2.2 Takaya–Nakamura (TN01) wave activity flux

The Takaya-Nakamura (2001) wave activity flux (TN01 flux) has been used for determining the horizontal propagation of quasi-stationary Rossby waves in a zonally varying background flow (Takaya and Nakamura, 2001). The zonal ($F_x$) and meridional ($F_y$) components of TN01 are

https://doi.org/10.5194/egusphere-2025-2990
Preprint. Discussion started: 1 August 2025


defined as:

$$F_x = \frac{p}{2|U^*|r_0{}^2}\left(\frac{U}{\cos\varphi}\left(\left(\frac{\partial\psi'}{\partial\lambda}\right)^2 - \psi'\frac{\partial^2\psi'}{\partial\lambda^2}\right) + V\left(\frac{\partial\psi'}{\partial\lambda}\frac{\partial\psi'}{\partial\varphi} - \psi'\frac{\partial^2\psi'}{\partial\lambda\partial\varphi}\right)\right) \quad (3)$$

$$F_y = \frac{p}{2|U^*|r_0{}^2}\left(U\left(\frac{\partial\psi'}{\partial\lambda}\frac{\partial\psi'}{\partial\varphi} - \psi'\frac{\partial^2\psi'}{\partial\lambda\partial\varphi}\right) + V\cos\varphi\left(\left(\frac{\partial\psi'}{\partial\varphi}\right)^2 - \psi'\frac{\partial^2\psi'}{\partial\varphi^2}\right)\right) \quad (4)$$

where $\psi$ represents the stream function, $\lambda$ and $\varphi$ denote longitude and latitude, respectively, and $|U^*|$ is the magnitude of the total horizontal wind velocity. $U$ and $V$ are the climatological mean zonal and meridional wind components, respectively, while $p$ is pressure, and $r_0$ is Earth's radius.

### 2.2.3 Residual mean meridional circulation

The Transformed Eulerian–Mean (TEM) formulation suggested by Andrews and McIntyre (1976, 1978) has widely been employed for diagnosing the large–scale circulation in the middle atmosphere. Different from the conventional Eulerian mean, the TEM framework accounts for eddy heat and momentum fluxes, thereby providing a more accurate representation of actual mass transport. In particular, the residual mean meridional circulation encapsulates the net effect of both mean flow and wave–induced eddy motions, making it especially useful for diagnosing stratospheric processes, such as B-D circulation and wave–driven anomalies associated with stratospheric warming. It is defined as:

$$[v]^* = [v] - \frac{1}{\rho_0}\frac{\partial}{\partial z}\left(\frac{\rho_0\,[v'\theta']}{[\theta_z]}\right) \quad (5)$$

$$[w]^* = [w] - \frac{1}{r_0\cos\varphi}\frac{\partial}{\partial\varphi}\left(\frac{\cos\varphi\;[v'\theta']}{[\theta_z]}\right) \quad (6)$$

where $[v]^*$ and $[w]^*$ denote the meridional and vertical components of the residual velocity, respectively. The vertical coordinate $z$ is the log-pressure height defined as $z = -H\,log\frac{p}{1000\,hPa}$, where $H$ is the scale height (≈ 7 km). All other variables are consistent with those defined in Equations (1)-(4).

## 3 Impacts of ENSO on stratospheric atmospheric circulation

To quantify the cross–seasonal response of the Antarctic stratospheric circulation to ENSO,

https://doi.org/10.5194/egusphere-2025-2990
Preprint. Discussion started: 1 August 2025


we first correlate three ENSO indices: Niño4, Niño3.4, and Niño3, with the stratospheric temperature ($T_{10\text{-}30}$) and zonal wind ($U_{10\text{-}30}$) over Antarctica during the subsequent July–September period. Here, $T_{10\text{-}30}$ refers to the zonal-mean temperature averaged over 60 °S–90 °S at 10–30 hPa, and $U_{10\text{-}30}$ refers to the zonal-mean zonal wind averaged over 40 °S–50 °S at the same pressure levels (Table 1).

**Table 1.** Correlation coefficients between Niño4, Niño3.4 and Niño3 indices and zonal-mean temperature index ($T_{10\text{-}30}$) averaged over 60 °S to 90 °S as well as zonal wind index ($U_{10\text{-}30}$) averaged over 40 °S to 50 °S at 10–30 hPa.

| | $T_{10\text{-}30}$_Jul | $T_{10\text{-}30}$_Aug | $T_{10\text{-}30}$_Sep | $U_{10\text{-}30}$_Jul | $U_{10\text{-}30}$_Aug | $U_{10\text{-}30}$_Sep |
|---|---|---|---|---|---|---|
| Niño4_Sep | 0.37*** | 0.36** | 0.32** | -0.26* | -0.31** | -0.30** |
| Niño4_Oct | 0.35** | 0.36** | 0.34** | -0.22 | -0.29* | -0.32** |
| Niño4_Nov | 0.37*** | 0.40*** | 0.32** | -0.22 | -0.32** | -0.31** |
| Niño4_Dec | 0.38*** | 0.42*** | 0.35** | -0.24 | -0.37*** | -0.34** |
| Niño4_Jan | 0.42*** | 0.43*** | 0.30** | -0.31** | -0.40*** | -0.33** |
| Niño4_Feb | 0.41*** | 0.41*** | 0.31** | -0.30** | -0.38*** | -0.32** |
| Niño4_Mar | 0.38*** | 0.39*** | 0.30** | -0.23 | -0.34** | -0.28* |
| | | | | | | |
| Niño3.4_Sep | 0.34** | 0.26* | 0.20 | -0.20 | -0.21 | -0.20 |
| Niño3.4_Oct | 0.32** | 0.27* | 0.24 | -0.19 | -0.21 | -0.23 |
| Niño3.4_Nov | 0.34** | 0.29* | 0.23 | -0.20 | -0.23 | -0.23 |
| Niño3.4_Dec | 0.37*** | 0.31** | 0.25* | -0.19 | -0.24 | -0.23 |
| Niño3.4_Jan | 0.38*** | 0.32** | 0.21 | -0.24 | -0.26* | -0.21 |
| Niño3.4_Feb | 0.38*** | 0.32** | 0.21 | -0.25* | -0.26* | -0.21 |
| Niño3.4_Mar | 0.36** | 0.35** | 0.25* | -0.23 | -0.28* | -0.23 |
| | | | | | | |
| Niño3_Sep | 0.33** | 0.22 | 0.14 | -0.18 | -0.17 | -0.16 |
| Niño3_Oct | 0.31** | 0.21 | 0.18 | -0.17 | -0.16 | -0.18 |
| Niño3_Nov | 0.32** | 0.23 | 0.19 | -0.17 | -0.18 | -0.18 |
| Niño3_Dec | 0.35** | 0.25* | 0.21 | -0.16 | -0.18 | -0.18 |
| Niño3_Jan | 0.35** | 0.25* | 0.16 | -0.20 | -0.19 | -0.16 |
| Niño3_Feb | 0.36** | 0.27* | 0.16 | -0.20 | -0.19 | -0.15 |
| Niño3_Mar | 0.29* | 0.31** | 0.20 | -0.21 | -0.23 | -0.19 |

Note: Colors and asterisks denote statistical significance: red with *** for the 99 % confidence level, bule with ** for 95 %, and magenta with * for 90 %.

Among the three indices, the Niño4 index has the largest correlation with Antarctic stratospheric circulations (Table 1). In particular, the Niño4 index exhibits a significantly positive

https://doi.org/10.5194/egusphere-2025-2990
Preprint. Discussion started: 1 August 2025


correlation with the subsequent July–September mean $T_{10-30}$ index, with correlations from September to March reaching the 95 % confidence level. Here, the largest correlation occurs during boreal winter (December–February), with correlation coefficients exceeding 0.30 at the 95 % confidence level ($R > 0.30$, $p < 0.05$). The January Niño4 index shows the highest correlation with August $T_{10-30}$ ($R > 0.43$, $p < 0.01$). Additionally, the December–February Niño4 index is significantly negatively correlated with the July–September $U_{10-30}$ index, with the largest negative correlation found between the January Niño4 and August $U_{10-30}$ ($R = -0.40$, $p < 0.01$). These correlations are consistent with stratospheric warming (cooling) and a weakened (strong) Stratospheric polar vortex (SPV) associated with warm (cold) central Pacific SSTs.

In comparison with Niño4, the Niño3.4 index has weaker correlations with stratospheric temperature and zonal wind. The January Niño3.4 has the highest correlation with July $T_{10-30}$ ($R \approx 0.38$, $p < 0.01$), while the correlation with September $T_{10-30}$ is not statistically significant. Similarly, its correlation with $U_{10-30}$ is weak, with only a marginally significant negative correlation between the January–March Niño3.4 index and July–August $U_{10-30}$ at the 90 % confidence level. However, the Niño3 index exhibits the weakest correlation with the polar stratosphere. While a moderate correlation with $T_{10-30}$ is observed during July–August, correlations in September are very weak and do not exceed the 90 % significance threshold.

We next examine the connection of ENSO phases in the preceding boreal winter with the Antarctic stratospheric circulation anomalies in July-September for 45 years 1980-2024 (Table 2). Here, we define a warm (cold) stratospheric year as the year when the July–September mean $T_{10-30}$ index is $\geq 0.5$ ($\leq -0.5$) standard deviations or when the $U_{10-30}$ index is $\leq -0.5$ ($\geq 0.5$) standard deviations. During the study period of 45 years, 14 are boreal winter El Niño years, of which 8 are followed by stratospheric warming events and 4 by cooling events, corresponding to an occurrence rate of 57 % and 28.5 %, respectively. Notably, 6 out of these 8 warming cases occur after central Pacific El Niño events. The remaining two cases, 2015/16 and 2023/24, are classified as eastern Pacific El Niño events, but are also accompanied by warm SSTs in the tropical central Pacific. By comparison, among 17 boreal winter La Niña years, 11 are followed by stratospheric cooling events and 4 by warming events, corresponding to occurrence rates of 65 % and 23.5 %, respectively. Of the 13 ENSO–neutral years, four are associated with stratospheric warming events and another four with cooling events, indicating no clear preference for either condition during neutral years.

https://doi.org/10.5194/egusphere-2025-2990
Preprint. Discussion started: 1 August 2025


**Table 2.** Relationship between ENSO phases in the preceding boreal winter and Antarctic stratospheric temperature (AST) anomalies during July–September for the 45-year period (1980–2024).

| Year (DJF) | Event Type | AST Anomalies | Year (DJF) | Event Type | AST Anomalies |
|---|---|---|---|---|---|
| 1980–1981 | Neutral | Cold (C) | 2002–2003 | El Niño (CP) | C |
| 1981–1982 | Neutral | C | 2003–2004 | Neutral | W |
| 1982–1983 | El Niño (EP) | C | 2004–2005 | El Niño (CP) | W |
| 1983–1984 | La Niña | Warm(W) | 2005–2006 | La Niña | C |
| 1984–1985 | La Niña | Normal (N) | 2006–2007 | El Niño (CP) | W |
| 1985–1986 | Neutral | W | 2007–2008 | La Niña | C |
| 1986–1987 | El Niño (CP) | C | 2008–2009 | La Niña | C |
| 1987–1988 | El Niño (CP) | W | 2009–2010 | El Niño (CP) | W |
| 1988–1989 | La Niña | C | 2010–2011 | La Niña | C |
| 1989–1990 | Neutral | N | 2011–2012 | La Niña | W |
| 1990–1991 | Neutral | C | 2012–2013 | Neutral | N |
| 1991–1992 | El Niño (CP) | W | 2013–2014 | Neutral | N |
| 1992–1993 | Neutral | N | 2014–2015 | El Niño (CP) | C |
| 1993–1994 | Neutral | N | 2015–2016 | El Niño (EP) | W |
| 1994–1995 | El Niño (CP) | N | 2016–2017 | La Niña | W |
| 1995–1996 | La Niña | W | 2017–2018 | La Niña | C |
| 1996–1997 | Neutral | W | 2018–2019 | El Niño (CP) | W |
| 1997–1998 | El Niño (EP) | C | 2019–2020 | Neutral | C |
| 1998–1999 | La Niña | C | 2020–2021 | La Niña | C |
| 1999–2000 | La Niña | C | 2021–2022 | La Niña | C |
| 2000–2001 | La Niña | C | 2022–2023 | La Niña | N |
| 2001–2002 | Neutral | W | 2023–2024 | E (EP) | W |

| El Niño | La Niña | Neutral |
|---|---|---|
| Total: 14 | Total: 17 | Total: 13 |
| Warm (CP) / Cold | Warm / Cold | Warm / Cold |
| 8 (6) / 4 | 4 / 11 | 4 /4 |
| 57% / 28.5% | 23.5% / 65% | 31% /31% |

Correlation coefficients between the July–September mean $T_{10\text{-}30}$ index and the global SST field from the preceding boreal winter are shown in Figure 1a. The highest correlation coefficients are observed in the central Pacific, particularly over the Niño4 region. Additionally, significant positive correlations appear over the North Indian Ocean and the South Pacific, likely reflecting remote responses to ENSO (Alexander et al., 2002).

https://doi.org/10.5194/egusphere-2025-2990
Preprint. Discussion started: 1 August 2025


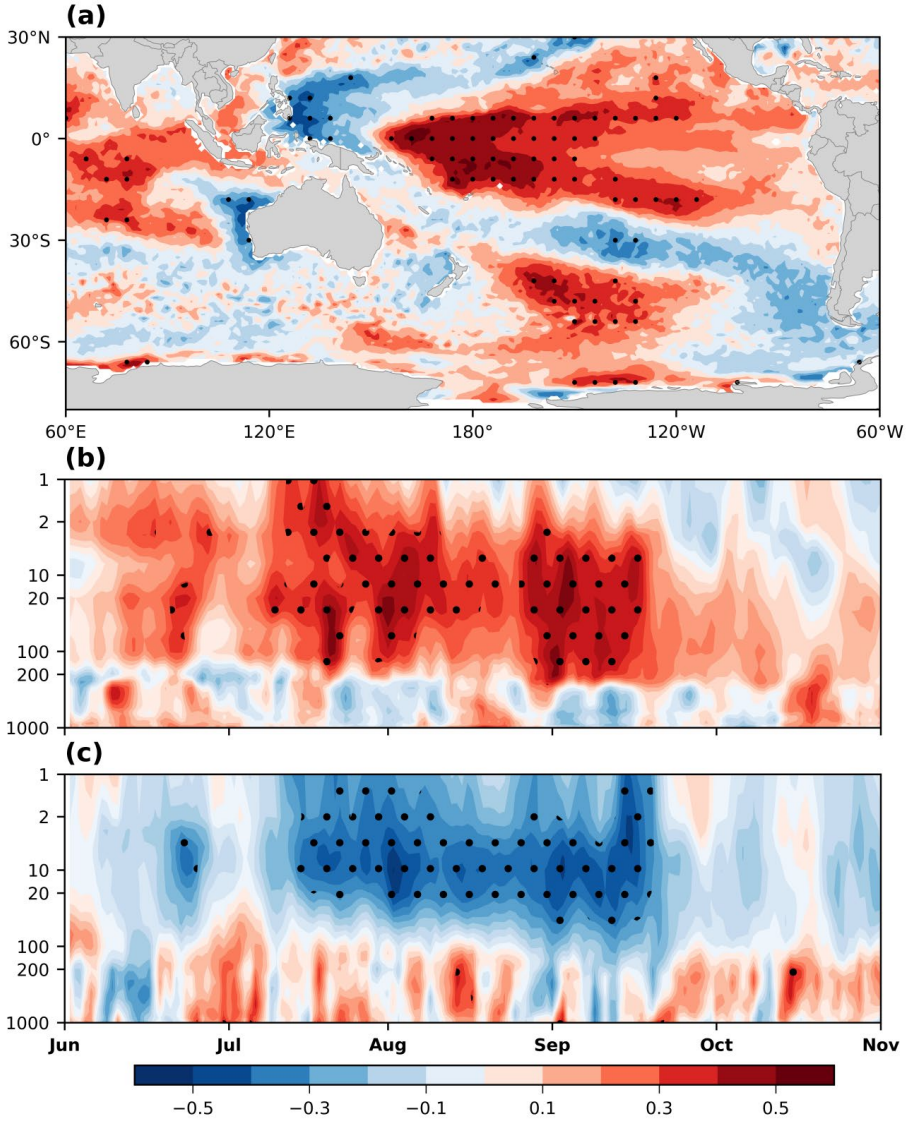


**Figure 1.** (a) Correlation coefficients between July–September mean $T_{10\text{-}30}$ index and January–March mean SST, (b) Correlation coefficients between December–February mean Niño4 index and daily Temperature averaged over 60 °S–90 °S, and (c) same as (b), but for zonal-mean zonal wind averaged over 40 °S–50 °S. Black dots represent the 95 % confidence level.

The most pronounced impacts of SSTs over the Niño4 region occur, however, above 100 hPa during the austral winter of the following year. Figs. 1b-c present the correlations between the boreal winter Niño4 index and the Antarctic daily zonal-mean temperature (averaged over 60 °S–

https://doi.org/10.5194/egusphere-2025-2990
Preprint. Discussion started: 1 August 2025


90 °S) and zonal-mean zonal wind (averaged over 40 °S–50 °S) from June to September of the following year. The Niño4 index exhibits significant positive correlations with stratospheric temperature and negative correlations with zonal wind during July–September, consistent with the stratospheric warming and weakened SPV.

To further examine the impacts of Niño4 SST anomalies on the stratospheric temperatures and the SPV, 17 warm years and 14 cold years according to ±0.5 standard of the Niño4 index are selected to calculate composite differences in zonal-mean temperature and zonal wind (Fig. 2). In June, warming is primarily observed in the upper polar stratosphere and the tropical troposphere, with the strongest signal at 1–5 hPa (Fig. 2a). As the season progresses, the warming intensifies and gradually propagates downward, with peak anomalies centered around ~60 °S in July–August (Figs. 2b–c). This warming reaches its maximum at 10 hPa around 80–90 °S in September (Fig. 2d).

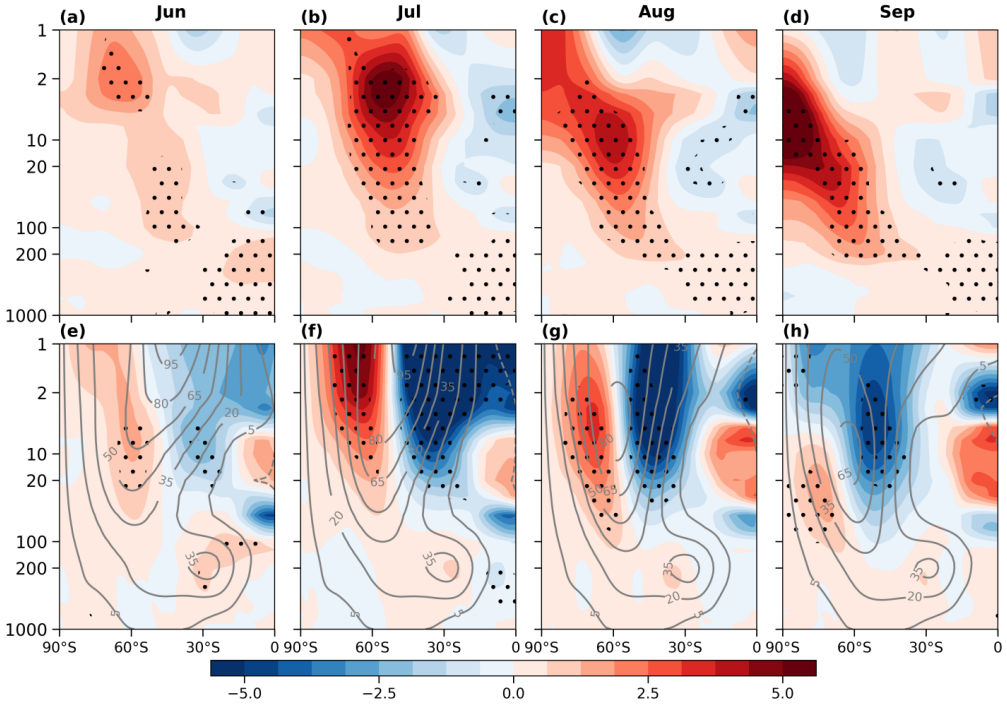


**Figure 2.** (a-d) Composite differences in zonal–mean temperatures between Niño4 warm and cold years from June to September, and (d-h) same as (a-d), but for zonal–mean zonal winds. The climatological mean of zonal-mean zonal winds is computed from 1991-2020 (contour, unit: m/s). Black dots indicate regions statistically

https://doi.org/10.5194/egusphere-2025-2990
Preprint. Discussion started: 1 August 2025


significant at the 95 % confidence level.

The stratospheric temperature anomalies are accompanied by a significant weakening of the polar stratospheric westerlies (Figs. 2e–h). Under climatological conditions, the polar night jet typically establishes and strengthens gradually from June to July, centered near 1 hPa and around 45 °S (Figs. 2e–f). The jet core then migrates poleward and downward in August and weakens in September (Figs. 2g–2h). However, during warm Niño4 years, anomalous easterlies emerge south of 45 °S as early as June (Fig. 2e) and progressively shift poleward from July to September, substantially weakening the climatological westerlies (Figs. 2f–h). Simultaneously, anomalous westerlies develop south of 60 °S, indicating a notable poleward contraction of the SPV (Figs. 2f–h). This pattern reflects a delayed yet robust stratospheric response to warm SST anomalies in the tropical central Pacific.

Figures 3a–b present time series of the boreal winter Niño4 index alongside the July–September mean $T_{10\text{-}30}$ and $U_{10\text{-}30}$ indices from 1981–2024. The Niño4 index exhibits a significant positive correlation with the $T_{10\text{-}30}$ index ($R = 0.43$, $p < 0.01$) (Fig. 3a) and a significant negative correlation with the $U_{10\text{-}30}$ index ($R = -0.38$, $p < 0.01$) (Fig. 3b), both are significant at the 99 % confidence level, indicating that a high (low) Niño4 index is typically associated with a warmer (colder) polar stratosphere and weaker (stronger) SPV. Notably, several prominent sudden stratospheric warming (SSW) events (e.g., 1988, 2019, 2024) coincide with positive Niño4 SSTs (Fig. 3a). The associated stratospheric changes also influence Antarctic ozone concentrations (Wang et al., 2025). For instance, TCO3 shows a strong positive correlation with both the $T_{10\text{-}30}$ index ($R = 0.56$, $p < 0.01$) and the boreal winter Niño4 index ($R = 0.36$, $p < 0.01$), both statistically significant at the 99 % confidence level (Fig. 3c). This suggests that warm (cold) Niño4 events enhance (suppress) poleward ozone transport, thereby increasing (decreasing) ozone concentrations over Antarctica.

https://doi.org/10.5194/egusphere-2025-2990
Preprint. Discussion started: 1 August 2025


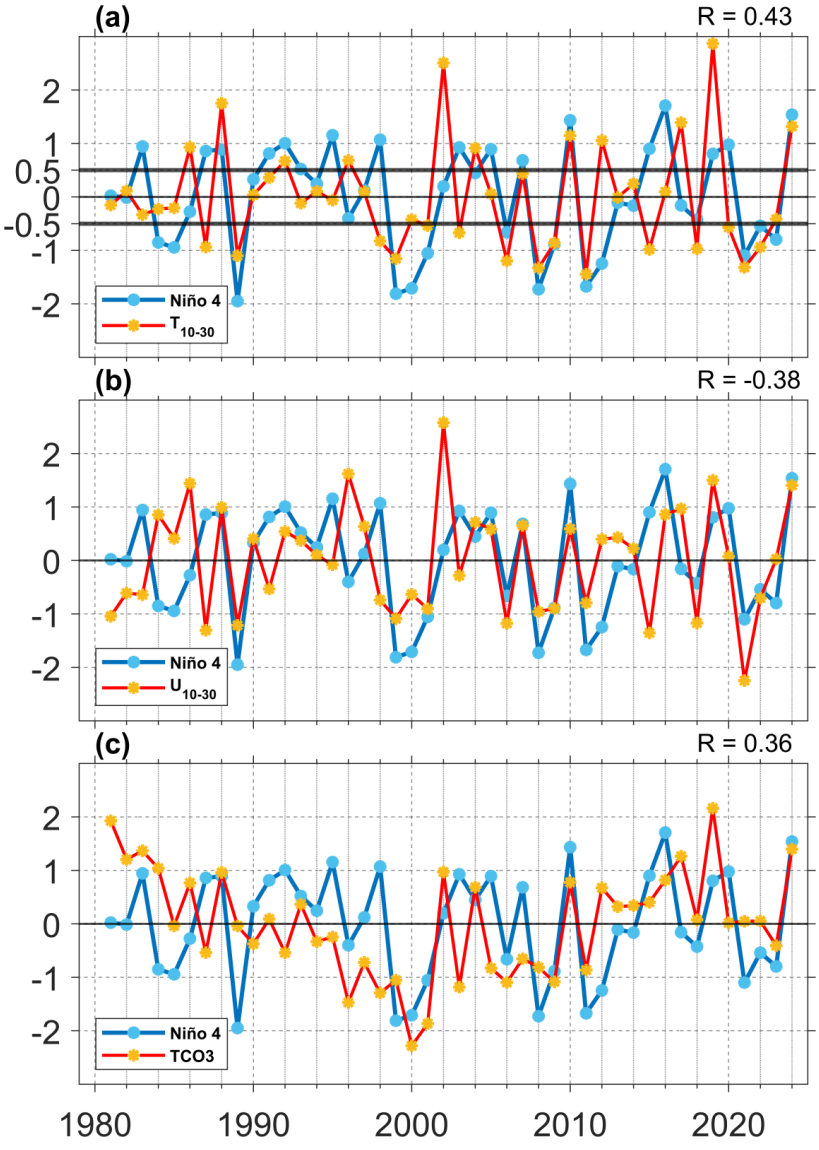


**Figure 3.** Time series of standardized Niño4 index (blue line), along with (a) July–September mean $T_{10\text{-}30}$ index (red line), (b) July–September mean $U_{10\text{-}30}$ index (red line, multiplied by -1), and (c) July–September mean TCO3 index (red line) from 1981 to 2024. R in the upper right corner denotes the correlation coefficient between the Niño4 index and the $T_{10\text{-}30}$, $U_{10\text{-}30}$, and TCO3 indices, respectively.

## 4 Effects of anomalous planetary waves

### 4.1 Stratospheric temperature and zonal wind

Previous studies suggested that polar stratospheric warming is primarily driven by the upward propagation of planetary waves from the troposphere, which disturb the SPV through wave–mean

https://doi.org/10.5194/egusphere-2025-2990
Preprint. Discussion started: 1 August 2025


flow interactions (Baldwin et al., 2021). To evaluate the effect of planetary wave activity on Antarctic stratospheric temperature anomalies during different Niño4 SST events, the composite differences of key atmospheric variables were calculated between warm and cold Niño4 years, averaged over consecutive three–month periods from January to September of the following year.

During the mature phase of El Niño (January–March), positive SST anomalies develop in the central and eastern Pacific (Fig. 4a). As SST increases, cumulus convection intensifies in the central Pacific (Fig. 4d), accompanied by a negative SLP anomaly and a positive geopotential height anomaly at 250 hPa over the tropical central Pacific, indicating a barotropic response (Figs. 4g,j). Furthermore, the convection anomaly triggers a southward–propagating teleconnection wave train at 250hPa, as suggested by the TN01 flux (Vector, Fig. 4j). This wave train, known as the PSA teleconnection (Mo and Higgins, 1998), features a positive geopotential height anomaly over the southeastern Pacific (near 110 °W, 60 °S) and a negative anomaly over the southwestern Pacific (near 150 °W, 40 °S) (Fig. 4j). The warm Niño4 SSTs and their associated convection responses over the tropical central Pacific persist into April–June (Figs. 4b,e,h,k). Although the amplitude of the high and low-pressure centers over the southeastern and southwestern Pacific weakens, the PSA wave train remains active (Fig. 4k). By July–September (austral winter), the warm Niño4 SSTs and their associated barotropic responses begin to dissipate (Figs. 4c,i,l). However, despite the weakening of tropical convention (Fig. 4f), it is strong enough to sustain a weak mid-latitude PSA wave train, maintaining a persistent positive geopotential height anomaly over the southeastern Pacific and a negative anomaly over the South Atlantic, as indicated by the TN01 flux (Fig. 4l).

https://doi.org/10.5194/egusphere-2025-2990
Preprint. Discussion started: 1 August 2025


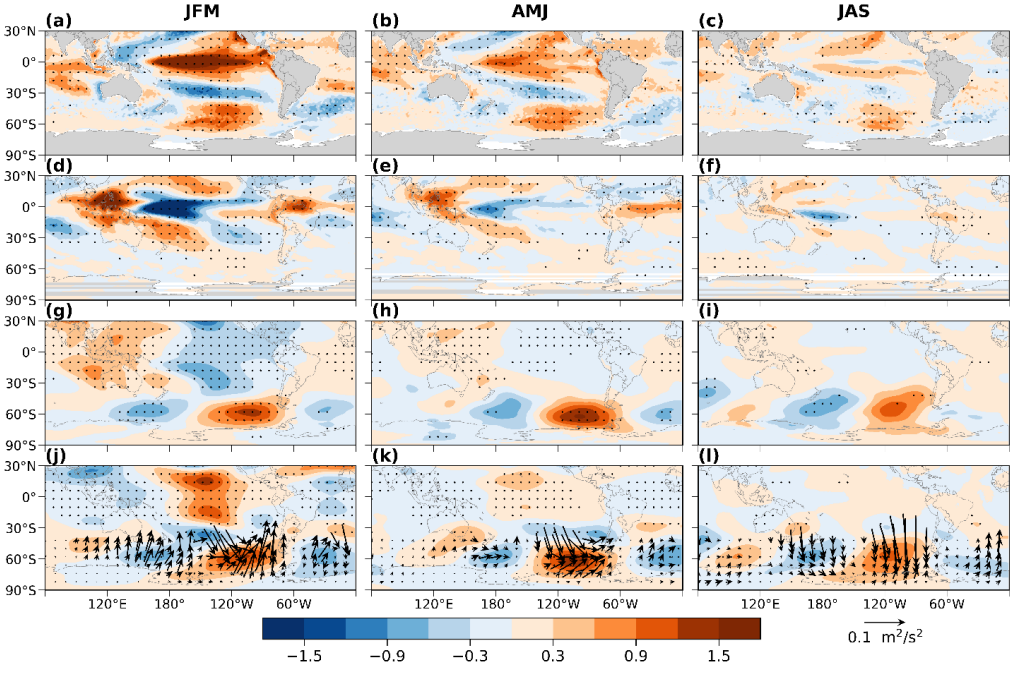


**Figure 4.** (a-c) Composite differences of SST (shaded, unit: K) for three-month means of: (a) January–March, (b) April–June and (c) July–September, (d-f) same as (a-c), but for OLR (shaded, unit: $1.5*10e^6$ w/m$^2$), (g-i) same as (a-c), but for SLP (shaded, unit: 300 Pa), and (j-l) same as (a-c), but for geopotential heights at 250 hPa (shaded, unit: 5 dagpm) and TN01 flux (vector, unit: 0.1 m$^2$/s$^2$). Black dots indicate regions statistically significant at the 95 % confidence level.

The geopotential height anomaly extends into the lower stratosphere and remains statistically significant at 100 hPa (Fig. 5). The climatological geopotential height at 100 hPa is characterized by a wave-1 pattern, featuring a positive center over the South Pacific and a negative center over the Atlantic Ocean and Indian Ocean sectors (contour lines in Fig. 5). During January-February-March (JFM) (austral summer), geopotential height anomalies associated with warm central Pacific SSTs form a wave train, with a positive center over the southeastern Pacific and two negative centers over the southwestern Pacific and the southern Atlantic (Fig. 5a). However, this pattern does not align well with the climatological wave-1 structure, indicating a displacement of the wave pattern (Fig. 5d). Moreover, the anomalous wave-1 centers at high latitudes are not statistically significant (Fig. 5d). Although the wave-1 component of the geopotential height shows a westward tilt with altitude and broadly resembles with the climatological structure, this alignment is only statistically significant below 500 hPa (Fig. 5g). As a result, planetary waves are not substantially

https://doi.org/10.5194/egusphere-2025-2990
Preprint. Discussion started: 1 August 2025


amplified in the lower stratosphere, primarily due to the prevailing easterly winds in the upper stratosphere over Antarctica in JFM (contours, Fig. 6a), which inhibit upward propagation of planetary waves (Baldwin et al., 2021). This is further supported by the E–P flux vectors, which show that planetary wave propagation is largely confined below 50 hPa in the mid– and low–latitudes (Fig. 6a).

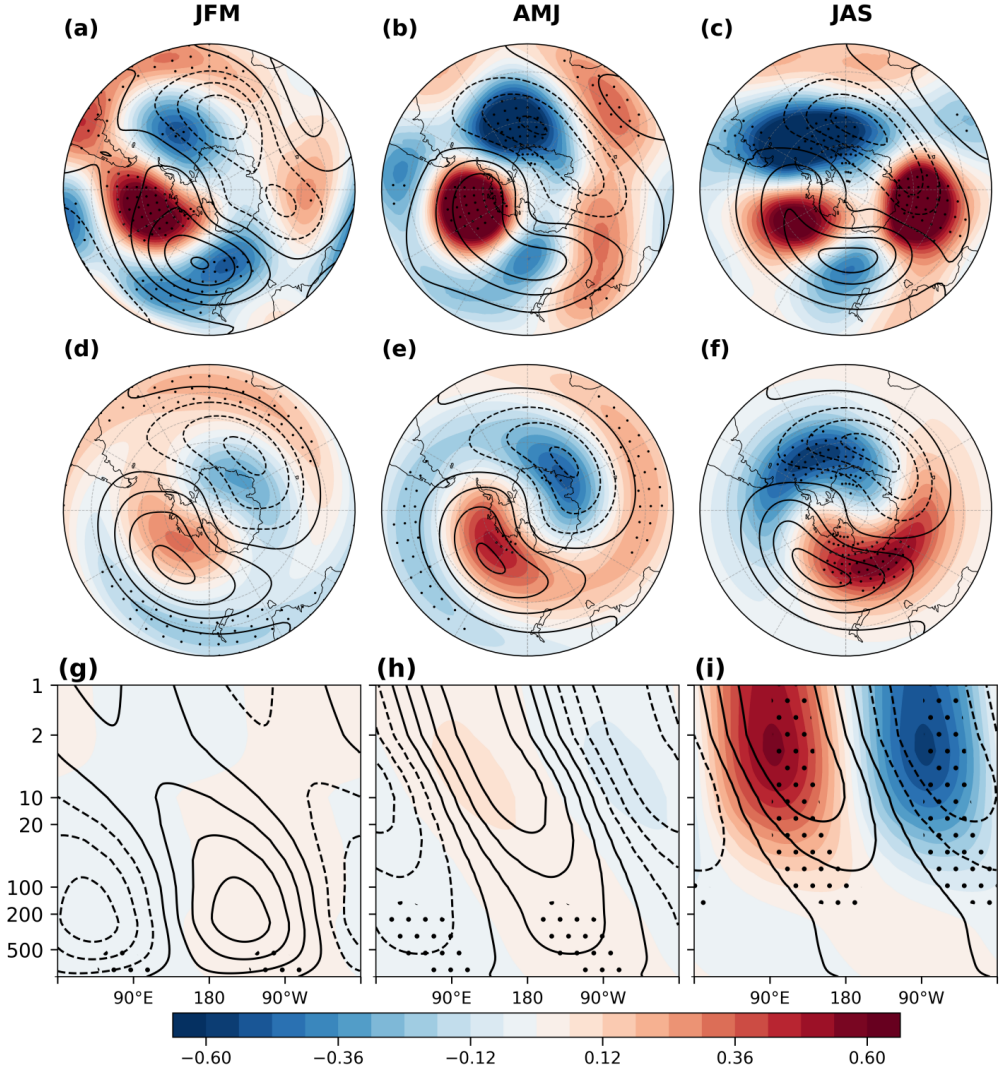


**Figure 5.** (a-c) Same as Figure 4, but for geopotential heights at 100 hPa (shaded, unit: 5 dagpm), where the climatological geopotential heights at 100 hPa is calculated from 1991–2020 (contours, unit: dagpm), (d-f) same as (a-c), but for wave-1 of geopotential heights at 100 hPa, and (g-i) same as (a-c), but for wave-1 of geopotential

https://doi.org/10.5194/egusphere-2025-2990
Preprint. Discussion started: 1 August 2025


heights at 1000–1hPa averaged from 45 °S–75 °S (shaded, unit: 30 dagpm). Black dots indicate the regions statistically significant at the 95 % confidence level.

During April-May-June (AMJ), the positive geopotential height center over the southeastern Pacific and the negative center over the southern Atlantic become more pronounced (Fig. 5b), aligning more closely with the climatological wave-1 pattern (Fig. 5e). This alignment contributes to a westward tilt of the geopotential height field with altitude (Fig. 5h). However, this vertical tilt is only statistically significant below 100 hPa (Fig. 5h). During this period, stratospheric zonal winds gradually transition to a westerly regime, but large portions of the upper polar stratosphere continue to experience weak westerlies or even easterlies (contours, Fig. 6b). As a result, a significant portion of the planetary waves are refracted equatorward, and their ability to disturb the polar stratosphere remains limited (Fig. 6b).

https://doi.org/10.5194/egusphere-2025-2990
Preprint. Discussion started: 1 August 2025


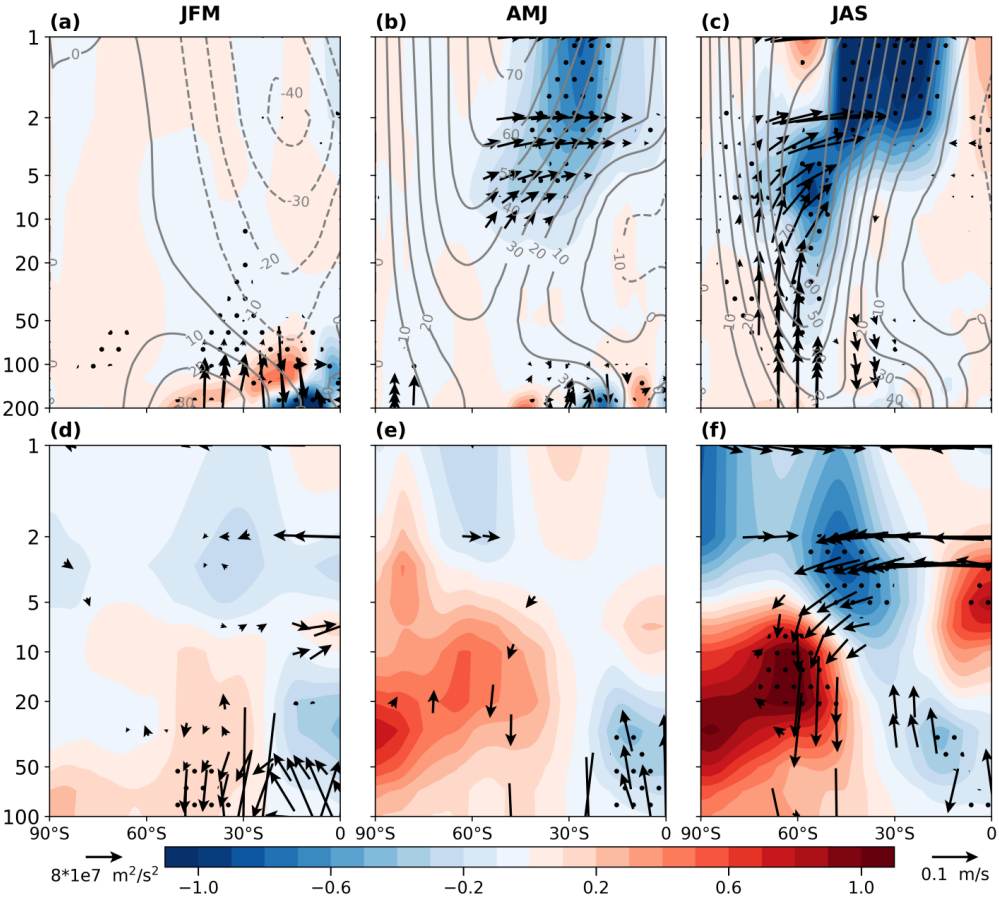


**Figure 6.** (a-c) Same as Figure 4, but for E-P flux (vector: $m^2/s^2$) and its divergence (shaded, unit: 60 m/s/day), where the climatological zonal-mean zonal winds are calculated from 1991–2020 (contours, unit: m/s), and (d-f) same as (a-c), but for the residual mean circulation (vector, unit: m/s) and ozone mass mixing ratio (shaded, unit: $3\times1e^{-6}$ kg/kg). Black dots denote regions statistically significant at the 95 % confidence level.

During July-August-September (JAS), the geopotential height centers over the southeastern Pacific weaken, while the positive center over the southern Indian Ocean strengthens significantly (Fig. 5c). This spatial pattern enhances the climatological wave-1 trough and ridge structure (Fig. 5f) and exhibits a westward tilt of the geopotential height field with altitude, which becomes statistically significant in the stratosphere (Fig. 5i). During this period, the polar regions enter the polar night, with minimal solar heating, which increases baroclinicity in the mid– and high–latitudes. The stratosphere becomes fully dominated by strong westerly winds, creating favorable conditions for the upward propagation of planetary waves into the polar stratosphere (contour lines,

https://doi.org/10.5194/egusphere-2025-2990
Preprint. Discussion started: 1 August 2025


Fig. 6c). Through wave–mean flow interactions, these waves induce strong wave convergence, which perturbs the SPV and leads to significant polar stratospheric warming (Fig. 6c).

This relationship is reversed under cold Niño4 SST conditions. Specifically, when cold SST anomalies occur in the central tropical Pacific, planetary wave activity and their associated disturbances to the stratosphere are suppressed, leading to polar stratospheric cooling and a strengthening SPV.

### 4.2 Mid-latitude sea-air interactions

#### 4.2.1 Ocean responses

Niño4 SSTs influence mid-latitude ocean temperatures through atmospheric teleconnections. During JFM, a positive Niño4 SSTs trigger a PSA teleconnection pattern, resulting in a high-pressure anomaly centered near 110 °W, 60 °S over the southeastern Pacific (Figs. 4j and 7g). The associated poleward surface winds and adiabatic subsidence warm the lower troposphere (Figs. 7a,d), while the ocean gains heat, as indicated by the negative net heat flux anomaly, defined as the sum of latent and sensible heat fluxes, long-wave radiant and short-wave radiant heating (Fig. 7m), leading to a localized SST warming (Fig. 7g). Simultaneously, there is a modest reduction in SIC in the Amundsen and Ross Seas (Fig. 7j).

https://doi.org/10.5194/egusphere-2025-2990
Preprint. Discussion started: 1 August 2025


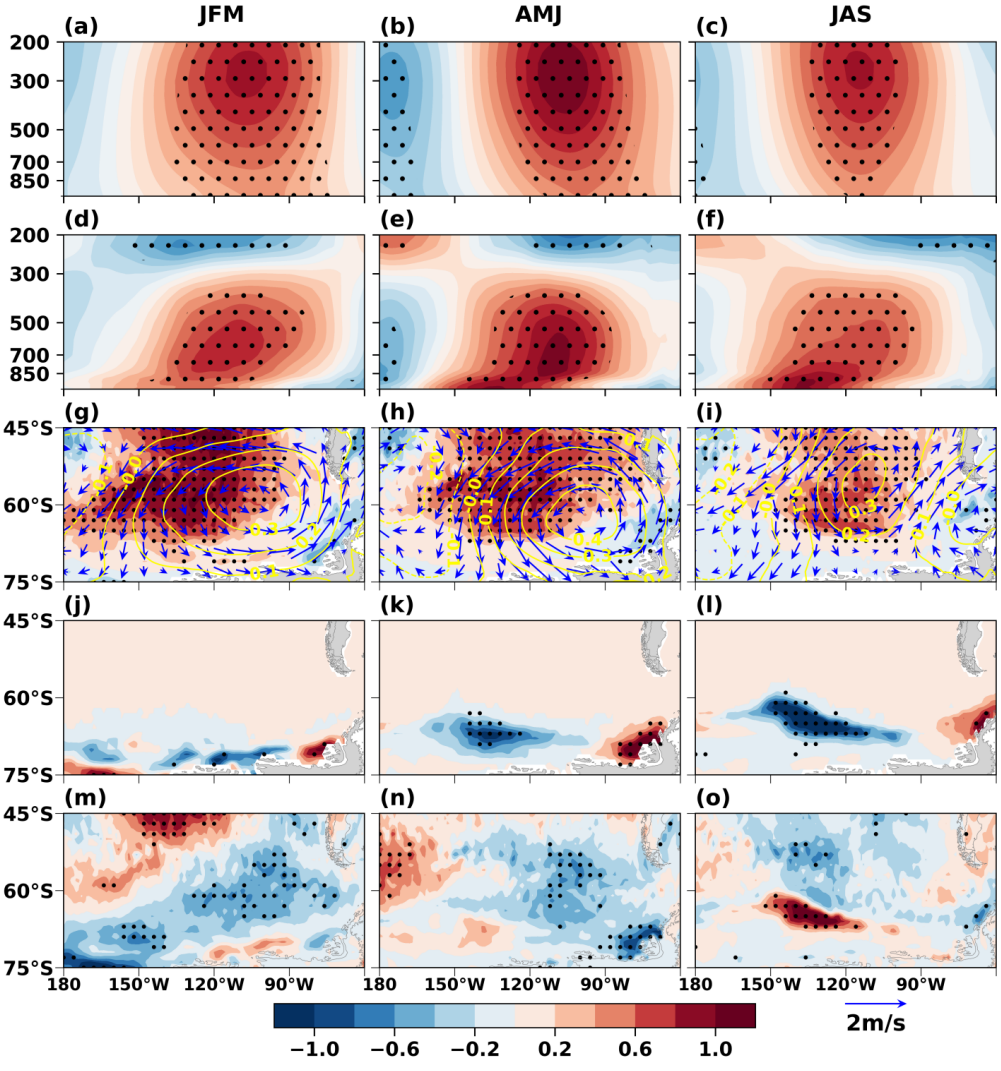


**Figure 7.** (a-c) Same as Figure 4, but for geopotential heights (shaded, unit: 5 dagpm) averaged over 45 °S–75 °S, (d-f) same as (a-c), but for temperatures (shaded, unit: K) averaged over 45 °S–75 °S, (g-i) same as Figure 4, but for SST (shaded, unit: K), SLP (contours, unit: 1000 Pa), and 10-meter winds (vector, unit: 2 m/s), (j-l) same as (a-c), but for SIC (unit: 100 %), and (m-o) same as (a-c), but for net upward total heat flux ( the sum of net turbulence heat flux, upward long-wave heat flux and net downward short-wave heat flux, shaded, unit: 3 W/m$^2$). Black dots denote regions statistically significant at the 95 % confidence level.

A similar pattern persists during AMJ (Figs. 7b,e). The PSA pattern associated with warm Niño4 SSTs remains evident (Fig. 4k), although the area of negative net heat flux contracts (Fig. 7n), and continues to support elevated SSTs in the southeastern Pacific through ongoing sea-air

https://doi.org/10.5194/egusphere-2025-2990
Preprint. Discussion started: 1 August 2025


heat exchange (Fig. 7h). As a result, SIC in the Amundsen and the Ross Seas declines further (Fig. 7k). Additionally, sustained tropospheric warming enhances geopotential height anomalies in both the troposphere and lower stratosphere (Figs. 7b,e).

#### 4.2.2 Ocean feedback to the atmosphere

While the tropospheric warming center is located between 500 hPa and 850 hPa during JFM and AMJ, the maximum warming shifts below 850 hPa in JAS, suggesting an increased influence from the ocean surface (Figs. 7d-f). During the JAS, the Niño4 SST warming weakens (Fig. 4c), indicating a reduced influence of equatorial central-Pacific SSTs. Nevertheless, due to the ocean's large heat capacity, warm SSTs in the southeastern Pacific persist (Fig. 7i), although with reduced amplitude, implying that the accumulated heat is gradually being released (Fig. 7o). A pronounced positive geopotential height anomaly associated with the PSA pattern also remains over this region (Fig. 4l), likely sustained by local sea–air interactions.

In JAS, surface heat flux is largely associated with sea-ice loss in the Amundsen and Ross Seas (Figs. 7l,o). Specifically, the sustained warm SSTs drive substantial sea-ice loss, which reduces surface albedo and enhances short-wave radiation absorption, further accelerating sea-ice decline (Figs. 7i,l,o). During this stage, although the negative net heat flux anomalies persist north of 60 °S, their intensity is relatively weak. In contrast, significant oceanic heat is released to the atmosphere in the regions where sea-ice has retreated (Fig. 7o), warming the lower troposphere (Fig. 7f) and sustaining the positive geopotential height anomaly by lifting isobaric surfaces (Fig. 7c). Notably, while net heat flux is dominated by ocean heat uptake during JFM and AMJ, the influence of sea-ice loss becomes predominant in JAS, resulting in net heat release from the ocean to the atmosphere (Figs. 7m-o). This positive feedback reinforces the Southern Hemisphere zonal-wave pattern and amplifies the planetary wave anomalies (Zi et al., 2025).

### 4.3 Ozone transport

The enhanced planetary wave activity associated with the Niño4 SST warming not only warms the polar stratosphere but also significantly alters the B–D residual circulation and polar ozone transport (Wang et al., 2025). Figures 6d–6f present the composite differences in the zonal-mean residual circulation and ozone mass mixing ratio between warm and clod Niño4 years, each averaged over three–month periods from January to September of the following year.

During JFM, convective anomalies in the tropical Pacific Ocean drive changes in the residual

https://doi.org/10.5194/egusphere-2025-2990
Preprint. Discussion started: 1 August 2025


circulation (Fig. 4d), resulting in decreases to the ozone mass mixing ratio in the tropical lower stratosphere and increased values in the mid–latitude lower stratosphere (Fig. 6d). However, upward–propagating planetary waves are largely confined below 50 hPa in the mid– and low–latitudes (Fig. 6a), strengthening the residual circulation primarily north of 60 °S. As a result, ozone transport to higher altitudes and into the polar region remains limited (Fig. 6d). In AMJ, although convective anomalies in the tropical Pacific Ocean persist and wave activity increases in the upper stratosphere (Fig. 6b), many of the waves are refracted equatorward, resulting in only modest polar ozone transport (Fig. 6e). In JAS, however, upward–propagating planetary waves are strongly refracted toward mid– and high–latitudes, enhancing the residual circulation and promoting both poleward and upward ozone transport (Fig. 6f). The increased poleward ozone transport enhances solar radiation absorption, playing an important role in the polar stratospheric warming through dynamical–chemical coupling (Solomon et al., 2016). In addition, adiabatic warming associated with descending air in the residual circulation further contributes to the stratospheric warming over the polar region.

## 5 Multivariate regression model

The preceding analyses reveal that boreal winter Niño4 SSTs exert a significant lagged influence on the Antarctic stratospheric circulation and ozone transport during the subsequent austral winter. This finding has important implications for the seasonal prediction of stratospheric variability. However, although the boreal winter Niño4 index is significantly correlated with July–September mean $T_{10\text{-}30}$ index, it accounts for only 18.5 % of the variance in stratospheric temperature ($R^2 = 0.185$). To enhance predictive skill, additional predictors must be incorporated.

Previous studies found that The PSA teleconnection associated with Niño4 SSTs is a key mechanism influencing the Antarctic stratosphere. The PSA pattern is represented by the second EOF mode of monthly SLP anomalies (Fig. 8a). The corresponding PSA index is defined as the time series of this EOF mode. During boreal winter, the PSA index is significantly correlated with the Niño4 index ($R = 0.40$, $p < 0.01$), suggesting that Niño4 SSTs modulate the PSA pattern. Furthermore, correlating the PSA index from December to the following September with the July–September mean $T_{10\text{-}30}$ index shows that the June PSA index exhibits the strongest relationship (R

https://doi.org/10.5194/egusphere-2025-2990
Preprint. Discussion started: 1 August 2025


= 0.47, $p < 0.01$). Interestingly, the June PSA index is only moderately correlated with the winter Niño4 index ($R = 0.28$, $p < 0.1$), indicating that it partially captures independent variability.

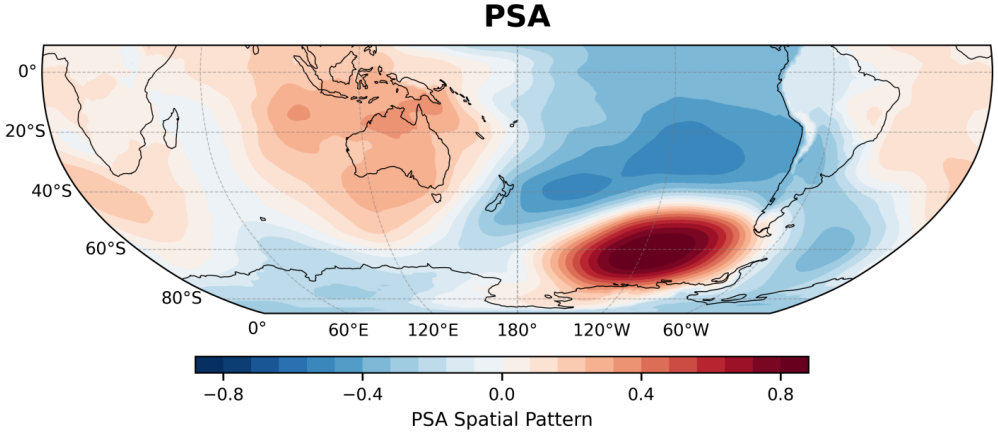


**Figure 8.** PSA teleconnection pattern represented by the second EOF mode of monthly SLP.

The loss of sea-ice in the Amundsen and Ross Seas, along with the warm South Pacific SSTs pattern, can also influence stratospheric temperatures during July–September through sea-air interactions. The strongest correlation between the July–September mean $T_{10\text{-}30}$ and Antarctic SIC in the Amundsen and Ross Seas (averaged over 180 °W–90 °W) occurs in May–June ($R = -0.43$, $p < 0.01$). However, the May–June SIC index is also significantly correlated with the preceding winter Niño4 index ($R = -0.42$, $p < 0.01$). Therefore, both Antarctic SIC anomalies and Antarctic stratospheric temperature variations may be driven by the influence of boreal winter Niño4 SSTs, implying that sea-ice loss itself might not be the primary driver of stratospheric warming.

In addition, a South Pacific SST index ($SST_{SP}$) was defined as the regional mean SST over 160 °W–130 °W and 30 °S–60 °S. Correlation analysis shows that the June $SST_{SP}$ index has the strongest correlation with the July–September mean $T_{10\text{-}30}$ index ($r = 0.31$, $p < 0.05$).

As a result, a multivariate linear regression (MLR) model is used to quantitatively assess the linear relationship between the stratospheric temperature index ($T_{10\text{-}30}$) and potential predictors including the Niño4 index, PSA index, South Pacific SST index ($SST_{SP}$), and SIC index. We have

$$T_{10-30} = \beta_0 + \beta_1\ Niño4 + \beta_2\ PSA + \beta_3\ SST_{SP} + \beta_4\ SIC + \varepsilon \qquad (7)$$

https://doi.org/10.5194/egusphere-2025-2990
Preprint. Discussion started: 1 August 2025


where $\beta_0$ is the intercept, $\beta_1$, $\beta_2$, $\beta_3$, $\beta_4$ are the regression coefficients associated with each predictor, and $\varepsilon$ denotes the residual error term. Prior to the regression analysis based on Eq. (7), all input time series are standardized. The regression analysis is performed using MATLAB's fitlm function, which yields estimates of regression coefficients, standard errors, t-statistics, and p-values, along with overall model diagnostics, such as the coefficient of determination ($R^2$) and the F-statistic. To evaluate the significance of individual predictors, three confidence levels are adopted: 90 %, 95 %, and 99 %, corresponding to p-value thresholds of 0.1, 0.05, and 0.01, respectively. Predictors with p-values below these thresholds are considered statistically significant. The overall performance and goodness-of-fit of the model are assessed using the $R^2$ metric.

To predict the July–September mean $T_{10\text{-}30}$ index, the boreal winter Niño4 ($Niño4_{\_DJF}$) index, the June PSA ($PSA_{\_Jun}$) index, the June $SST_{SP}$ ($SST_{SP\_Jun}$) index, and the May–June mean SIC ($SIC_{\_MJ}$) index are used as predictors in Eq. (7). We yield

$$T_{10-30} = 0.2765\, Niño4_{\_DJF} + 0.2879\, PSA_{\_Jun} + 0.1176\, SST_{SP\_Jun} - 0.1347\, SIC_{\_MJ} + \varepsilon \qquad (8)$$

with $\beta_0 = 0$. This four–variable linear regression model yields a coefficient of determination ($R^2$) of 0.35, indicating that the predictors collectively explain approximately 35 % of the variance in the July–September mean $T_{10\text{-}30}$ index. The model's F-statistic is 5.24 with a corresponding p-value of 0.00178, which is significant at the 99 % confidence level.

Among the predictors, $Niño4_{\_DJF}$ and $PSA_{\_Jun}$ exhibit statistically significant regression coefficients ($p = 0.0201$ and $p = 0.0065$, respectively), confirming their primary roles in modulating stratospheric temperature. In contrast, $SST_{SP\_Jun}$ and $SIC_{\_MJ}$ are not individually significant ($p = 0.41$ and $p = 0.40$, respectively), suggesting that their linear contributions are relatively weak. Nevertheless, the regression coefficients of $SST_{SP\_Jun}$ and $SIC_{\_MJ}$ indices are positive (0.1176) and negative (-0.1347), respectively, implying potential nonlinear effects associated with South Pacific SST increases and sea-ice loss over the Amundsen and Ross Seas. For instance, while the changes in $SST_{SP\_Jun}$ and $SIC_{\_MJ}$ are linked to high pressure anomalies associated with the PSA, increases in SST and reductions in SIC, in turn, reinforce these high pressure anomalies (Fig. 7c), highlighting a nonlinear feedback process.

To assess model performance, the regression–based fitted index (referred to as $NP_{fit}$) was compared with observed July–September mean $T_{10\text{-}30}$, $U_{10\text{-}30}$, and TCO3 (Fig. 9). The $NP_{fit}$ index

https://doi.org/10.5194/egusphere-2025-2990
Preprint. Discussion started: 1 August 2025


shows significant correlation with observed values for $T_{10\text{-}30}$ ($R = 0.59$, $p < 0.01$), $U_{10\text{-}30}$ ($R = -0.56$, $p < 0.01$), and TCO3 ($R = 0.39$, $p < 0.01$), all of which exceed the corresponding correlation values ($R = 0.4$, -0.38 and 0.36) obtained using Niño4 index alone (Fig. 2). While the boreal winter Niño4 index can serve as a useful predictor of Antarctic stratospheric variability, incorporating additional indices, namely the June PSA, June South Pacific SST, and May–June mean SIC over the Amundsen and Ross Seas indices, enhances predictive skill. This underscores the importance of both tropical forcing and extratropical feedback processes in modulating polar stratospheric circulation.

https://doi.org/10.5194/egusphere-2025-2990
Preprint. Discussion started: 1 August 2025


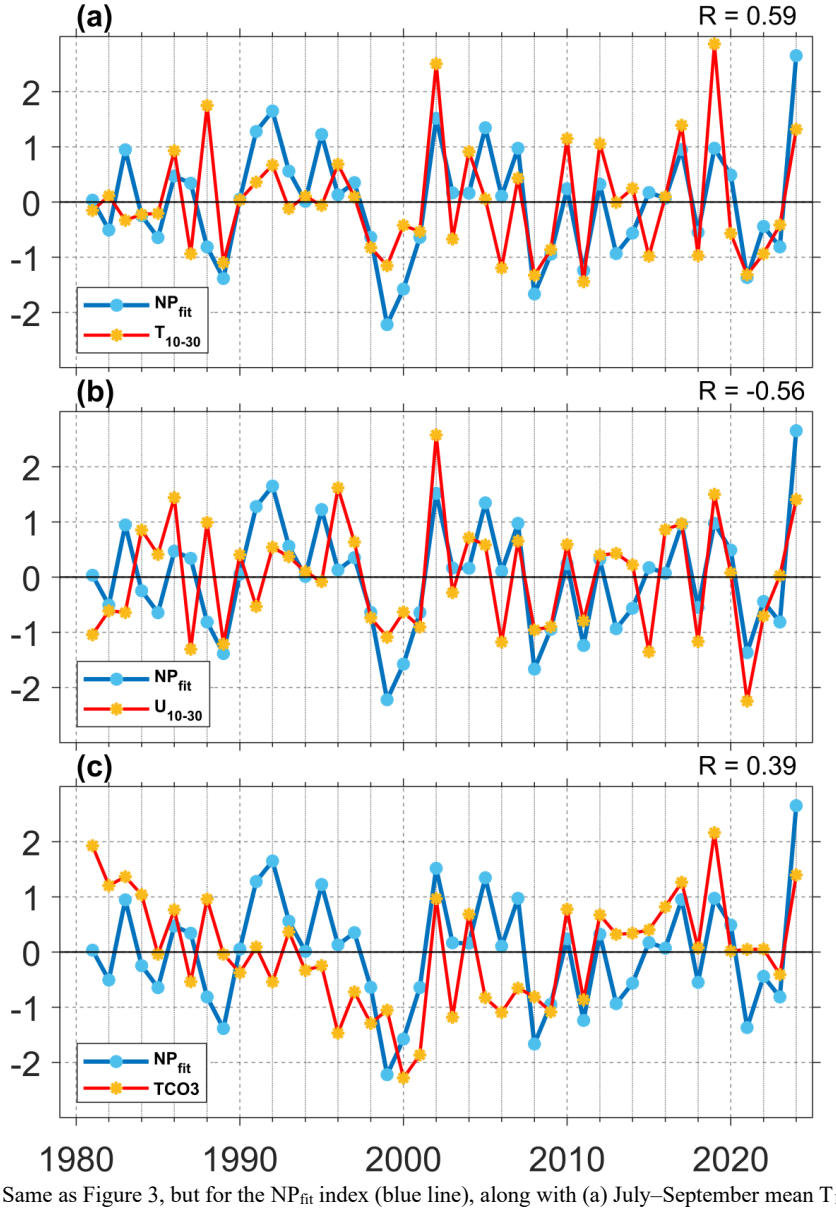


**Figure 9.** Same as Figure 3, but for the $NP_{fit}$ index (blue line), along with (a) July–September mean $T_{10\text{-}30}$ index (red line), (b) July–September mean $U_{10\text{-}30}$ index (red line, multiplied by -1), and (c) July–September mean TCO3 index (red line) from 1981 to 2024. R in the upper right corner is the correlation coefficient between $NP_{fit}$ index and $T_{10\text{-}30}$, $U_{10\text{-}30}$, and TCO3 indices, respectively.

## 6 Conclusions and discussions

The cross–seasonal influence of the El Niño–Southern Oscillation (ENSO) on Antarctic stratospheric circulation was investigated in this study using ERA5 reanalysis of 45 years (1980–

https://doi.org/10.5194/egusphere-2025-2990
Preprint. Discussion started: 1 August 2025


2024). Our analysis revealed that sea surface temperature (SST) anomalies have a significant impact on the stratospheric temperatures. Specifically, warm (cold) SST anomalies (SSTs) in the Niño4 region (Central Pacific) during boreal winter are followed by significantly warming (cooling) of the Antarctic stratosphere in the subsequent austral winter (July–September), accompanied by a weakening (strengthening) of the stratospheric polar vortex (SPV). Among the ENSO indices (Niño3, Niño3.4, Niño4), the boreal winter Niño4 index exhibits the strongest and most robust correlation with the July–September polar stratospheric temperature ($T_{10\text{-}30}$) index, reaching $R \approx 0.43$ ($p < 0.01$). In contrast, correlations with Niño3.4 and Niño3 indices (Eastern Pacific) are substantially weaker, suggesting that Niño4 SSTs are the primary drivers of the observed Antarctic stratospheric responses.

The underlying dynamics involve the Pacific–South America (PSA) teleconnection pattern triggered by Niño4 SSTs and mediated through wave–mean flow interactions. During boreal winter, warm SSTs in the Niño4 region enhance convection near the dateline, exciting a Rossby wave train that propagates poleward and eastward across the Southern Hemisphere. This wave activity generates a positive geopotential height anomaly over the southeastern South Pacific and a negative anomaly over the South Atlantic, reinforcing the climatological wave-1 ridge and trough structure. As the seasonal transition into austral summer and winter progresses, the Antarctic stratospheric circulation shifts toward a more westerly regime, creating favorable conditions for planetary waves into the polar stratosphere. The convergence of Eliassen–Palm (E–P) fluxes, followed by wave breaking, induces stratospheric warming and a deceleration of the SPV.

It was also found that warm SSTs in the South Pacific and sea-ice loss over the Amundsen and Ross Seas can reinforce the mid and high latitudes zonal wave train through sea–air interactions. Specially, PSA teleconnection associated with Niño4 warming drives ocean heat uptake and rising SSTs in the southeast Pacific from January-March to April-June. With progression of seasons, this remote forcing weakens during the June-September, a local sea-air feedback becomes dominant, persistent warm waters accelerate sea-ice melt, and the subsequent oceanic heat release sustains the atmospheric high pressure anomaly, thereby strengthening the planetary wave anomaly.

Furthermore, stronger planetary wave anomalies induced by warm Niño4 SSTs were found to play a crucial role in modulating Antarctic ozone transport. These anomalous waves enhance the residual circulation, facilitating the ozone transport from the tropics to the polar stratosphere and

https://doi.org/10.5194/egusphere-2025-2990
Preprint. Discussion started: 1 August 2025


leading to elevated ozone concentrations over Antarctica. The increased ozone concentrations enhance ultraviolet absorption, further amplifying stratospheric warming. Simultaneously, a warmer stratosphere inhibits the formation of polar stratospheric clouds (PSCs), thereby suppressing the heterogeneous chemical reactions responsible for ozone depletion and mitigating Antarctic ozone loss (Solomon et al., 2016).

A multivariate regression statistical model was used in this study to determine the linear relationship between stratospheric temperature variations and Niño4 SST. The Niño4 index alone accounts for approximately 18 % of the variance in July–September polar stratospheric temperatures. However, when the June PSA index, June South Pacific SST ($SST_{SP}$) index, and the May–June mean Antarctic sea-ice concentration (SIC) index are included as additional predictors, the explained variance nearly doubles to 35 %. This highlights the combined importance of both tropical forcing and mid–latitude atmospheric responses in stratospheric temperature predictability. Such forecasts based on this multivariate regression model can provide lead times of up to 1–6 months for anticipating potential stratospheric warming events and assessing the risk of ozone depletion during the austral winter.

Nonetheless, a substantial portion of stratospheric variability remains unexplained. This reflects the influence of atmospheric internal dynamics, as well as contributions from other drivers such as the Quasi–Biennial Oscillation (QBO), solar activity, and mid–latitude tropospheric wave sources. Additional predictors may be identified through a range of approaches, including numerical modeling, machine learning, and causal inference.

**Code and data availability.**

The ERA5 reanalysis data are available from the European Centre for Medium–Range Weather Forecasts at Hersbach et al. (2023). Niño4 index came from National Oceanic and Atmospheric Administration (https://psl.noaa.gov/data/timeseries/month/DS/Nino4/, https://psl.noaa.gov/data/timeseries/month/DS/Nino3/, and https://psl.noaa.gov/data/timeseries/month/DS/Nino34/). The code used in this article is accessible from the corresponding author.

**Author contributions**

https://doi.org/10.5194/egusphere-2025-2990
Preprint. Discussion started: 1 August 2025


YZ, ZL, JS, and ZX contributed to the conceptualization of the study. YZ designed the methodology, developed the software, performed the validation, formal analysis, investigation, data curation, and visualization. JS, GL, and ZX were responsible for funding acquisition, project administration, and providing the necessary resources. The work was supervised by ZL, JS, GL, WP, and ZX. YZ prepared the original manuscript with contributions from ZL, JS, WP, and ZX. All authors contributed to the review and editing of the final manuscript.

**Competing interests**

The contact author has declared that none of the authors has any competing interests.

**Acknowledgments**

The research was supported by the National Natural Science Foundation of China (42394123 and 42394122), "Transforming Climate Action" program (TCA-LRP-20240B-1.1-WP6JS) led by Dalhousie University, Canada, Natural Sciences and Engineering Research Council of Canada to JS (NSERC, Grant NOs: 217081), and the China Scholarship Council (CSC, 202306340119). We also appreciate all the support provided by the Department of Oceanography, Dalhousie University.

**Financial support**

This research was supported by the National Natural Science Foundation of China (42394123 and 42394122), the "Transforming Climate Action" program (TCA-LRP-20240B-1.1-WP6JS), Natural Sciences and Engineering Research Council of Canada to JS (NSERC, Grant NOs: 217081), and the China Scholarship Council (CSC, 202306340119).

https://doi.org/10.5194/egusphere-2025-2990
Preprint. Discussion started: 1 August 2025


## References

Alexander, M.A., Bladé, I., Newman, M., Lanzante, J. R., Lau, N. C., and Scott, J. D.: The Atmospheric Bridge: The Influence of ENSO Teleconnections on Air–Sea Interaction over the Global Oceans, Journal of Climate, 15, 2205–2231, https://doi.org/10.1175/1520-0442(2002)015<2205:tabtio>2.0.co;2, 2002.

Andrews, D. G. and Mcintyre, M. E.: An exact theory of nonlinear waves on a Lagrangian-mean flow, Journal of Fluid Mechanics, 89, 609–646, https://doi.org/10.1017/s0022112078002773, 1978.

Andrews, D. G. and McIntyre, M. E.: Planetary Waves in Horizontal and Vertical Shear: The Generalized Eliassen-Palm Relation and the Mean Zonal Acceleration, Journal of the Atmospheric Sciences, 33, 2031–2048, https://doi.org/10.1175/1520-0469(1976)033<2031:pwihav>2.0.co;2, 1976.

Andrews, D. G., Holton, J. R., and Leovy, C. B.: Middle atmosphere dynamics, Academic Press, 115, 421–422, https://doi.org/10.1002/qj.49711548612, 1987.

Baldwin, M. P. and Dunkerton, T. J.: Stratospheric Harbingers of Anomalous Weather Regimes, Science, 294, 581–584, https://doi.org/10.1126/science.1063315, 2001.

Baldwin, M. P., Ayarzagüena, B., Birner, T., Butchart, N., Butler, A. H., Charlton‐Perez, AndrewJ., Domeisen, DanielaI. V., Garfinkel, ChaimI., Garny, H., Gerber, EdwinP., Hegglin, MichaelaI., Langematz, U., and Pedatella, NicholasM.: Sudden Stratospheric Warmings, Reviews of Geophysics, 59, https://doi.org/10.1029/2020rg000708, 2021.

Bamston, A. G., Chelliah, M., and Goldenberg, S. B.: Documentation of a highly ENSO‐related sst region in the equatorial pacific: Research note, Atmosphere-Ocean, 35, 367–383, https://doi.org/10.1080/07055900.1997.9649597, 1997.

Barriopedro, D. and Calvo, N.: On the Relationship between ENSO, Stratospheric Sudden Warmings, and Blocking, Journal of Climate, 27, 4704–4720, https://doi.org/10.1175/jcli-d-13-00770.1, 2014.

Butler, A. H. and Polvani, L. M.: El Niño, La Niña, and stratospheric sudden warmings: A reevaluation in light of the observational record, Geophysical Research Letters, 38, n/a-n/a, https://doi.org/10.1029/2011gl048084, 2011.

Domeisen, D. I. V., Garfinkel, C. I., and Butler, A. H.: The Teleconnection of El Niño Southern Oscillation to the Stratosphere, Reviews of Geophysics, 57, 5–47, https://doi.org/10.1029/2018rg000596, 2019.

Esler, J. G., Polvani, L. M., and Scott, R. K.: The Antarctic stratospheric sudden warming of 2002: A self‐tuned resonance?, Geophysical Research Letters, 33, https://doi.org/10.1029/2006gl026034, 2006.

Evtushevsky, O. M., Kravchenko, V. O., Hood, L. L., and Milinevsky, G. P.: Teleconnection between the central tropical Pacific and the Antarctic stratosphere: spatial patterns and time lags, Climate Dynamics, 44, 1841–1855, https://doi.org/10.1007/s00382-014-2375-2, 2015.

Fogt, R. L., Bromwich, DavidH., and Hines, KeithM.: Understanding the SAM influence on the South Pacific ENSO teleconnection, Climate Dynamics, 36, 1555–1576,

https://doi.org/10.5194/egusphere-2025-2990
Preprint. Discussion started: 1 August 2025


https://doi.org/10.1007/s00382-010-0905-0, 2011.

Garfinkel, C. I. and Hartmann, D. L.: Different ENSO teleconnections and their effects on the stratospheric polar vortex, Journal of Geophysical Research: Atmospheres, 113, https://doi.org/10.1029/2008jd009920, 2008.

Grassi, B., Redaelli, G., and Visconti, G.: Tropical SST Preconditioning of the SH Polar Vortex during Winter 2002, Journal of Climate, 21, 5295–5303, https://doi.org/10.1175/2008jcli2136.1, 2008.

Hersbach, H., Bell, B., Berrisford, P., Biavati, G., Horányi, A., Muñoz Sabater, J., Nicolas, J., Peubey, C., Radu, R., Rozum, I., Schepers, D., Simmons, A., Soci, C., Dee, D., and Thépaut, J.-N.: ERA5 hourly data on pressure levels from 1940 to present, Copernicus Climate Change Service (C3S) Climate Data Store (CDS), Dataset, https://doi.org/10.24381/cds.bd0915c6, 2023a.

Hersbach, H., Bell, B., Berrisford, P., Biavati, G., Horányi, A., Muñoz Sabater, J., Nicolas, J., Peubey, C., Radu, R., Rozum, I., Schepers, D., Simmons, A., Soci, C., Dee, D., and Thépaut, J.-N.: ERA5 hourly data on single levels from 1940 to present, Copernicus Climate Change Service (C3S) Climate Data Store (CDS), Dataset, https://doi.org/10.24381/cds.adbb2d47, 2023b.

Hu, Y. and Fu, Q.: Stratospheric warming in Southern Hemisphere high latitudes since 1979, Atmospheric Chemistry and Physics, 9, 4329–4340, https://doi.org/10.5194/acp-9-4329-2009, 2010.

Hurwitz, M. M., Newman, P. A., Oman, L. D., and Molod, A. M.: Response of the Antarctic Stratosphere to Two Types of El Niño Events, Journal of the Atmospheric Sciences, 68, 812–822, https://doi.org/10.1175/2011jas3606.1, 2011a.

Hurwitz, M. M., Song, I.-S., Oman, L. D., Newman, P. A., Molod, A. M., Frith, S. M., and Nielsen, J. E.: Response of the Antarctic stratosphere to warm pool El Niño Events in the GEOS CCM, Atmospheric Chemistry and Physics, 11, 9659–9669, https://doi.org/10.5194/acp-11-9659-2011, 2011b.

Ineson, S. and Scaife, A. A.: The role of the stratosphere in the European climate response to El Niño, Nature Geoscience, 2, 32–36, https://doi.org/10.1038/ngeo381, 2009.

Karpetchko, A., Kyrö, E., and Knudsen, B. M.: Arctic and Antarctic polar vortices 1957 ‐ 2002 as seen from the ERA ‐ 40 reanalyses, Journal of Geophysical Research: Atmospheres, 110, https://doi.org/10.1029/2005jd006113, 2005.

Kim, B.-M., Choi, H., Kim, S.-J., and Choi, W.: Amplitude-dependent relationship between the Southern Annular Mode and the El Niño Southern Oscillation in austral summer, Asia-Pacific Journal of Atmospheric Sciences, 53, 85–100, https://doi.org/10.1007/s13143-017-0007-6, 2017.

Kuroda, Y., Deushi, M., and Shibata, K.: Role of solar activity in the troposphere ‐ stratosphere coupling in the Southern Hemisphere winter, Geophysical Research Letters, 34, https://doi.org/10.1029/2007gl030983, 2007.

L'Heureux, M. L. and Thompson, D. W. J.: Observed Relationships between the El Niño–Southern

https://doi.org/10.5194/egusphere-2025-2990
Preprint. Discussion started: 1 August 2025


Oscillation and the Extratropical Zonal-Mean Circulation, Journal of Climate, 19, 276–287, https://doi.org/10.1175/jcli3617.1, 2006.

Laat, A. T. J., and Weele, M. V: The 2010 Antarctic ozone hole: Observed reduction in ozone destruction by minor sudden stratospheric warmings, Scientific Reports, 1, https://doi.org/10.1038/srep00038, 2011.

Lim, E. ‐P., Hendon, H. H., and Thompson, D. W. J.: Seasonal Evolution of Stratosphere ‐Troposphere Coupling in the Southern Hemisphere and Implications for the Predictability of Surface Climate, Journal of Geophysical Research: Atmospheres, 123, 12,002-12,016, https://doi.org/10.1029/2018jd029321, 2018.

Lim, E., Zhou, L., Young, G., Abhik, S., Rudeva, I., Hope, P., Wheeler, M. C., Arblaster, J. M., Hendon, H. H., Manney, G., Son, S., Oh, J., and Garreaud, R. D.: Predictability of the 2020 Strong Vortex in the Antarctic Stratosphere and the Role of Ozone, Journal of Geophysical Research: Atmospheres, 129, https://doi.org/10.1029/2024jd040820, 2024.

Lin, J. and Qian, T.: Impacts of the ENSO Lifecycle on Stratospheric Ozone and Temperature, Geophysical Research Letters, 46, 10646–10658, https://doi.org/10.1029/2019gl083697, 2019.

Lin, P., Fu, Q., and Hartmann, D. L.: Impact of Tropical SST on Stratospheric Planetary Waves in the Southern Hemisphere, Journal of Climate, 25, 5030–5046, https://doi.org/10.1175/jcli-d-11-00378.1, 2012.

Lin, P., Fu, Q., Solomon, S., and Wallace, J. M.: Temperature Trend Patterns in Southern Hemisphere High Latitudes: Novel Indicators of Stratospheric Change, Journal of Climate, 22, 6325–6341, https://doi.org/10.1175/2009jcli2971.1, 2009.

Ma, C., Yang, P., Tan, X., and Bao, M.: Possible Causes of the Occurrence of a Rare Antarctic Sudden Stratospheric Warming in 2019, Atmosphere, 13, 147, https://doi.org/10.3390/atmos13010147, 2022.

Manatsa, D. and Mukwada, G.: A connection from stratospheric ozone to El Niño-Southern Oscillation, Scientific Reports, 7, https://doi.org/10.1038/s41598-017-05111-8, 2017.

McPhaden, M. J., Zebiak, S. E., and Glantz, M. H.: ENSO as an Integrating Concept in Earth Science, Science, 314, 1740–1745, https://doi.org/10.1126/science.1132588, 2006.

Mo, K.C. and Higgins, R. W.: The Pacific–South American Modes and Tropical Convection during the Southern Hemisphere Winter, Monthly Weather Review, 126, 1581–1596, https://doi.org/10.1175/1520-0493(1998)126<1581:tpsama>2.0.co;2, 1998.

Niu, Y., Xie, F., and Wu, S.: ENSO Modoki Impacts on the Interannual Variations of Spring Antarctic Stratospheric Ozone, Journal of Climate, 36, 5641–5658, https://doi.org/10.1175/jcli-d-22-0826.1, 2023.

Polvani, L. M., Sun, L., Butler, A. H., Richter, J. H., and Deser, C.: Distinguishing Stratospheric Sudden Warmings from ENSO as Key Drivers of Wintertime Climate Variability over the North Atlantic and Eurasia, Journal of Climate, 30, 1959–1969, https://doi.org/10.1175/jcli-d-16-0277.1, 2017.

Rao, J., Garfinkel, C. I., Ren, R., Wu, T., and Lu, Y.: Southern Hemisphere Response to the Quasi-

https://doi.org/10.5194/egusphere-2025-2990
Preprint. Discussion started: 1 August 2025


Biennial Oscillation in the CMIP5/6 Models, Journal of Climate, 36, 2603–2623, https://doi.org/10.1175/jcli-d-22-0675.1, 2023.

Rayner, N. A., Parker, D. E., Horton, E. B., Folland, C. K., Alexander, L. V., Rowell, D. P., Kent, E. C., and Kaplan, A.: Global analyses of sea surface temperature, sea ice, and night marine air temperature since the late nineteenth century, Journal of Geophysical Research: Atmospheres, 108, https://doi.org/10.1029/2002jd002670, 2003.

Shen, X., Wang, L., and Osprey, S.: Tropospheric Forcing of the 2019 Antarctic Sudden Stratospheric Warming, Geophysical Research Letters, 47, https://doi.org/10.1029/2020gl089343, 2020.

Silvestri, G. and Vera, C.: Nonstationary Impacts of the Southern Annular Mode on Southern Hemisphere Climate, Journal of Climate, 22, 6142–6148, https://doi.org/10.1175/2009jcli3036.1, 2009.

Singh, A. K. and Bhargawa, A.: Atmospheric burden of ozone depleting substances (ODSs) and forecasting ozone layer recovery, Atmospheric Pollution Research, 10, 802–807, https://doi.org/10.1016/j.apr.2018.12.008, 2019.

Solomon, S., Ivy, D. J., Kinnison, D., Mills, M. J., Neely, R. R., and Schmidt, A.: Emergence of healing in the Antarctic ozone layer, Science, 353, 269–274, https://doi.org/10.1126/science.aae0061, 2016.

Song, K. and Son, S.-W.: Revisiting the ENSO–SSW Relationship, Journal of Climate, 31, 2133–2143, https://doi.org/10.1175/jcli-d-17-0078.1, 2018.

Stone, K. A., Solomon, S., Thompson, D. W. J., Kinnison, D. E., and Fyfe, J. C.: On the Southern Hemisphere stratospheric response to ENSO and its impacts on tropospheric circulation, Journal of Climate, 35, 1963–1981, https://doi.org/10.1175/jcli-d-21-0250.1, 2022.

Takaya, K. and Nakamura, H.: A Formulation of a Phase-Independent Wave-Activity Flux for Stationary and Migratory Quasigeostrophic Eddies on a Zonally Varying Basic Flow, Journal of the Atmospheric Sciences, 58, 608–627, https://doi.org/10.1175/1520-0469(2001)058<0608:afoapi>2.0.co;2, 2001.

Thompson, D. W. J. and Solomon, S.: Interpretation of Recent Southern Hemisphere Climate Change, Science, 296, 895–899, https://doi.org/10.1126/science.1069270, 2002.

Thompson, D. W. J., Baldwin, M. P., and Solomon, S.: Stratosphere–Troposphere Coupling in the Southern Hemisphere, Journal of the Atmospheric Sciences, 62, 708–715, https://doi.org/10.1175/jas-3321.1, 2005.

Thompson, D. W. J., Solomon, S., Kushner, P. J., England, M. H., Grise, K. M., and Karoly, D. J.: Signatures of the Antarctic ozone hole in Southern Hemisphere surface climate change, Nature Geoscience, 4, 741–749, https://doi.org/10.1038/ngeo1296, 2011.

Trenberth, K. E.: The Definition of El Niño, Bulletin of the American Meteorological Society, 78, 2771 – 2777, https://doi.org/10.1175/1520-0477(1997)078<2771:tdoeno>2.0.co;2, 1997.

Wang, C.: A review of ENSO theories, National Science Review, 5, 813–825, https://doi.org/10.1093/nsr/nwy104, 2018.

Wang, Z., Zhang, J., Zhao, S., and Li, D.: The joint effect of mid-latitude winds and the westerly

https://doi.org/10.5194/egusphere-2025-2990
Preprint. Discussion started: 1 August 2025


quasi-biennial oscillation phase on the Antarctic stratospheric polar vortex and ozone, Atmospheric Chemistry and Physics, 25, 3465–3480, https://doi.org/10.5194/acp-25-3465-2025, 2025.

Yang, C., Li, T., Dou, X., and Xue, X.: Signal of central Pacific El Niño in the Southern Hemispheric stratosphere during austral spring, Journal of Geophysical Research: Atmospheres, 120, https://doi.org/10.1002/2015jd023486, 2015.

Zhang, R., Zhou, W., Tian, W., Zhang, Y., Liu, Z., and Cheung, P. K. Y.: Changes in the Relationship between ENSO and the Winter Arctic Stratospheric Polar Vortex in Recent Decades, Journal of Climate, 35, 5399–5414, https://doi.org/10.1175/jcli-d-21-0924.1, 2022.

Zi, Y., Long, Z., Sheng, J., Lu, G., Perrie, W., and Xiao, Z.: The Sudden Stratospheric Warming Events in the Antarctic in 2024, Geophysical Research Letters, 52, https://doi.org/10.1029/2025gl115257, 2025.

Zubiaurre, I. and Calvo, N.: The El Niño–Southern Oscillation (ENSO) Modoki signal in the stratosphere, Journal of Geophysical Research: Atmospheres, 117, https://doi.org/10.1029/2011jd016690, 2012.